Heating of underdense plasmas by intense short-pulse lasers

A. Djaoui[1] and A. A. Offenberger[2]
[1]*Rutherford Appleton Laboratory, Chilton, Didcot, Oxon, OX11 0QX, United Kingdom*
[2]*Department of Electrical Engineering, University of Alberta, Edmonton, Alberta, Canada T6G 2G7*
(Received 29 June 1994)

A one-dimensional model in cylindrical geometry which incorporates tunnel ionization, nonlinear inverse bremsstrahlung, and radial heat conduction is used to predict the spatial and temporal temperature distribution in an undercritical plasma irradiated axially by a short-pulse laser. Results from the calculation are compared to available experimental data using a 12 ps KrF laser and to previous work in a regime relevant to proposed recombination optical-field ionized xuv lasers in the transient regime, e.g., Li-like neon. The calculated temperature is too high for lasing to the ground state because of the large contribution from inverse bremsstrahlung for pulse lengths greater than 100 fs. It is shown that for small filaments, additional cooling by supersonic heat conduction on a few picosecond time scale could be used efficiently to generate inversion between excited states in the quasi-steady-state regime.

PACS number(s): 52.50.Jm, 52.65.+z, 42.55.Vc

I. INTRODUCTION

High power short-pulse lasers have opened up possibilities in high electric field interaction with matter. At intensities of about 10^{17} W/cm^2 it is possible to produce He-like neon, for example, through direct field induced ionization. It has been suggested that for short pulses ($\sim$100 fs) a plasma far from collisional equilibrium (with an electron thermal temperature much smaller than the ionization temperature) can be produced [1] by optical field ionization (OFI). Three-body recombination (preferentially into higher levels) following the short laser pulse can result in population inversion between excited states and between an excited and ground state of the ion. The transient inversion to the ground state can only last for a time determined by the filling of the ground state as a result of the radiative decay of the upper state ($\sim$1 ps) and is of current interest for short-pulse xuv lasers at short wavelengths. xuv lasing in plasmas produced by OFI is also potentially more efficient [2] than the conventional collisional and recombination x-ray lasers which rely on collisional ionization for the production of the appropriate ions [3]: in collisional ionization the bulk of the electron distribution is heated to the required temperature, but only a small fraction of these electrons (with energies of the order of the ionization and excitation energies) contribute to the ionization and excitation of the ions. As a consequence of their high efficiency xuv lasers based on OFI could be implemented on relatively small tabletop installations.

The transient x-ray laser scheme imposes severe requirements on plasma conditions and is not possible if the electron temperature is much higher than about one-tenth of the ionization energy of the recombining ions. For the Li-like neon scheme [2] the plasma must be almost completely ionized to the He-like stage following the passage of the optical laser pulse and the electron temperature no more than about 30 eV. Inversion between excited levels is also of current interest because additional cooling (by heat conduction) of a plasma filament allows less stringent requirements on the electron temperature. Processes that contribute to plasma heating include above threshold ionization (ATI) energy and nonlinear inverse bremsstrahlung (IB) [1]. Under special conditions stimulated Raman scattering [2], space charge effects associated with the laser ponderomotive force [4] and other collective mechanisms may be important. A consensus on the electron temperature of an optically ionized plasma has not been achieved: one study [4] predicted that a He-like neon plasma at an electron density of 10^{20} cm^{-3} irradiated with a 0.248 μm, 200 fs laser pulse at an intensity of 10^{18} W/cm^2 would have a residual temperature of about 10 eV, while another study [5] predicts a temperature of at least 200 eV. The validity of these calculations is difficult to assess without comparison to experimental measurements. Measurements of temperature in an OFI neon plasma have been reported recently [6]. These used Thomson scattering of the beam itself to infer the electron temperature during the laser pulse. The purpose of this paper is to present a detailed time dependent simulation of the ionization and heating of these gas targets. Nonlinear inverse bremsstrahlung and ATI heating as well thermal conduction cooling are taken into account. The densities covered in the experiment range from 1 to 100 Torr ($N_i = 3.3\times10^{16}$ to 3.3×10^{18} cm^{-3}). For the densities and laser intensities of interest in these experiments the heating contribution from stimulated processes is negligible. Ionization induced defocusing of the laser beam can also be neglected for the conditions of these experiments. The model is then extended to densities of interest to the xuv laser scheme ($N_i = 10^{19}$–10^{20} cm^{-3}) and shorter pulse length ($\sim$100 fs). Since our calculations do not include the contribution of stimulated processes to the heating, they only provide a lower limit to the electron temperatures.

In Sec. II we discuss the heating mechanisms and the heat conduction models used. The relative importance of the different processes as a function of electron density

and laser pulse length are pointed out. The simulation of the neon experiments using the 12 ps KrF laser [6] are presented in Sec. III. Electron temperatures for shorter pulses and higher densities relevant to xuv laser schemes are calculated in Sec. IV. A discussion of the results is presented in Sec. V.

II. DESCRIPTION OF PHYSICAL MODEL

The model is based on a one-dimensional Lagrangian hydrodynamic code coupled to a time dependent atomic model [7]. The atomic model was modified to include tunnel ionization and irradiation in the axial direction. At high laser intensities the rates for collisional processes are much smaller than OFI rates and only sequential tunnel ionization needs to be considered. In this situation ATI heating, nonlinear inverse bremsstrahlung, and a choice of flux limited diffusion and nonlocal heat conduction are also included in the model. The laser beam is assumed to have a Gaussian temporal profile and a Gaussian radial profile and is incident axially. Only radial gradients are taken into account as they are much more important than axial gradients within a distance of the order of a Rayleigh range ($z_R = 4\pi r_0^2/\lambda$) from the position of the focus where the measurements are made. λ is the laser wavelength and r_0 the beam radius (at $1/e$ of peak intensity).

A. Tunnel ionization rate and ATI heating

The most important ionization process for short-pulse high intensity laser-matter interaction is tunnel ionization. This is a very nonlinear process for which the rate rises very rapidly above a threshold intensity, which can be defined as the intensity for which the electric field depression of the atomic potential is equal to the binding energy of the electron [4,8]. Numerically this threshold intensity is approximately given by

$$I_{\text{thr}} = \frac{1.4\times 10^{14}}{Z^2}\left[\frac{U_i}{13.6}\right]^4 \text{W/cm}^2 , \tag{1}$$

where U_i is the ionization potential in eV and Z the residual charge of the ion seen by the photoelectron. Experiments [9] have shown good agreement with the generalized formula for the rate of tunnel ionization due to Ammosov, Delone, and Krainov [8]. The static field ionization rate is given by [4]

$$W = 1.61\omega_{\text{a.u.}}\frac{Z^2}{n^{4.5}}\left[10.87\frac{Z^3}{n^4}\frac{E_{\text{a.u.}}}{E}\right]^{2n-1.5} \times \exp\left[-\frac{2}{3}\frac{Z^3}{n^3}\frac{E_{\text{a.u.}}}{E}\right] \text{s}^{-1} , \tag{2}$$

where $\omega_{\text{a.u.}}$ is the atomic unit of frequency ($=4.1\times 10^{16}$ s^{-1}), E is the instantaneous laser electric field, $E_{\text{a.u.}}$ is the atomic field strength ($=5.1\times 10^9$ V/cm), and $n = Z(13.6/U_i)^{1/2}$.

The ATI heating can be attributed to the mismatch between the peak and the point in the laser cycle at which ionization occurs [10]. For a linearly polarized sinusoidal field an electron ionized at some arbitrary phase mismatch ϕ will acquire an average kinetic energy

$$E_k(\phi) = 2U_p\cos^2(\phi) , \tag{3}$$

where $U_p = e^2E_0^2/4m\omega^2$ is the ponderomotive potential, e and m are the electronic charge and mass, respectively, E_0 is the amplitude of the laser electric field, and ω is the laser angular frequency. The average ATI energy is obtained by multiplying by the rate of ionization and integrating over a laser cycle

$$E_{\text{ATI}} = \frac{\int W(\phi)E_k(\phi)d\phi}{\int W(\phi)d\phi} . \tag{4}$$

The ATI energy is dependent on the laser wavelength (proportional to λ^2) as well as the intensity at which the ionization occurs. For short-pulse lasers ionization occurs approximately at the threshold intensity (the exact value depends on the rise time of the pulse). The ATI energy is also strongly dependent on the polarization of the laser field and varies from approximately $0.1U_p$ for linearly polarization to $2U_p$ for circular polarization.

B. Nonlinear inverse bremsstrahlung

At low intensities the most important mechanism for heating plasmas with lasers is inverse bremsstrahlung or collisional absorption. The absorption is proportional to the electron ion collision frequency and to the laser intensity. At high laser intensities the electron velocity distribution is severely modified as a result of the oscillatory motion in the laser electric field. Consequently the electron ion collision frequency is reduced and the absorption becomes nonlinear and decreases with intensity. There is therefore an optimum intensity for efficient heating of a plasma by a laser when the thermal velocity [$v_{\text{th}} = (kT_e/m)^{1/2}$] is of the order of the oscillatory velocity ($v_{\text{os}} = eE_0/m\omega$) and is given approximately by

$$I_{\text{opt}} = 2.68\times 10^{12}T_e/\lambda^2 \text{ W/cm}^2 , \tag{5}$$

where T_e is in eV and λ in μm. The low intensity expression for the inverse bremsstrahlung absorption rate is given by the usual expression [11]

$$J = \frac{4}{3}\left[\frac{\pi}{2}\right]^{1/2}\frac{Z^{*2}N_eN_ie^6v_{\text{os}}^2\ln\Lambda}{\left[1-\frac{\omega_p^2}{\omega^2}\right]^{1/2}mv_{\text{th}}^3} \text{ erg s}^{-1}\text{cm}^{-3} , \tag{6}$$

where Z^* is the average ionization state, N_e and N_i are the electron and ion density, respectively, $\omega_p = (4\pi N_e e^2/m)^{1/2}$ is the plasma frequency, and the Coulomb logarithm term is defined in Ref. [11]. There is still no agreement on the high intensity expression. The first derivation of inverse bremsstrahlung at $v_{\text{os}} > v_{\text{th}}$ was given by Silin [12] and incorporates a correction to the logarithmic term proportional to $\ln(v_{\text{os}}/2v_{\text{th}}+1)$. A limited amount of tabular data was also given for intermediate intensities when $v_{\text{os}} \sim v_{\text{th}}$. A simple expression that interpolates between the low and high intensity cases and consists of replacing v_{th}^2 by $v_{\text{th}}^2 + v_{\text{os}}^2/6$ is given in Refs.

[13] and [14]. In Ref. [5], v_{th}^2 is replaced by $v_{th}^2+v_{os}^2/3$, while the Ref. [1] v_{th}^2 is replaced by $v_{th}^2+v_{os}^2$ and no changes to the logarithmic term are included. Some more recent work [15], which is used in our calculations, incorporates changes to the logarithmic term at high intensity and interpolates between the low and high intensity limits by effectively replacing v_{th}^2 by $v_{th}^2+v_{os}^2$. The high intensity expression is obtained by replacing $\ln\Lambda/v_{th}^3$ in Eq. (6) by

$$\frac{\frac{1}{4}\ln^2\left[1+\frac{v_{os}^2}{v_{th}^2}\right]+\ln\left[\frac{v_{os}^2}{v_{th}^2}+\exp(\frac{1}{3}\sqrt{\pi/2})\right]\ln\Lambda}{\frac{1}{3}\sqrt{\pi/2}(v_{os}^2+v_{th}^2)^{3/2}}.$$

Figure 1 shows the inverse bremsstrahlung heating rate per electron in He-like neon for a range of electron densities (10^{17}–10^{20} cm^{-3}) and a temperature of 30 eV as a function of laser intensity. The cycle averaged ATI energies for all ten-electrons of neon are also shown. It can be seen that the ATI energy increases with the ionization potential of the electron as a result of the increases in threshold intensity. For laser pulses with a duration of the order of 1 ps ATI heating is only significant compared to IB at the lowest electron densities. As the density increases, inverse bremsstrahlung increases (proportional to the electron density), while ATI remains constant. Above a few times 10^{19} W/cm^2 the ATI energy from the two last electrons in neon is much larger than the inverse bremsstrahlung heating rate even at the highest electron density shown. The intensity needed to remove these two last electrons in neon is, however, beyond the range considered in this work. The exact magnitude of each heating process depends not just on density, but also on intensity and pulse rise time and duration. A time dependent calculation of the ionization taking into account the temporal and spatial profiles of the laser beam is therefore necessary.

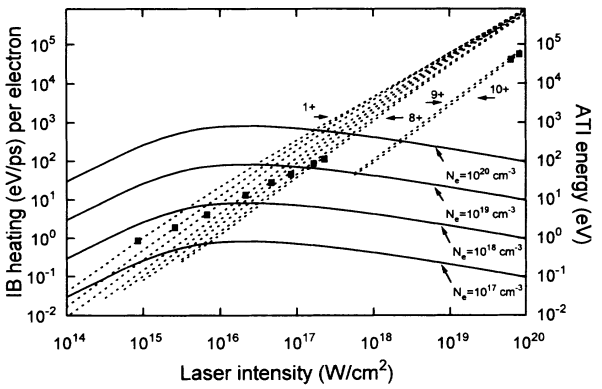

FIG. 1. Inverse bremsstrahlung (IB) heating rate per electron per picosecond as a function of intensity in He-like neon for a range of electron densities (full curves), at an electron temperature of 30 eV and a laser wavelength of 0.25 μm. The cycle averaged ATI energies for all ten electrons of neon are also shown (dotted curves). The ATI curves are labeled with the ionization stage under consideration (1+,8+,...). The full squares mark the value of the ATI energy at the threshold intensity as given by Eq. (1).

C. Electron heat conduction

For small laser focal spots and long pulses, thermal conduction cooling plays an important role in determining the electron temperature. In the diffusive limit, Spitzer and Harm [16] derive an expression for the thermal conductivity under the assumption that the electron mean free path is much smaller than the scale length of the temperature gradient ($L=T/|\nabla T|$) and that the electron distribution is locally a Maxwellian. When the gradient is so steep that L becomes smaller than the average mean free path or when the electron distribution deviates significantly from a Maxwellian, the Spitzer-Harm heat flux might exceed its physical upper limit, the free streaming limit given by $Q_f=fN_ekT_ev_{th}$, where f is of the order of unity. A full solution for the electron distribution function is complicated and a common remedy is to simply impose an upper limit on the local heat flux in order to avoid such nonphysical behavior. We will see that the calculated temperature will depend strongly on the value of the flux limiter used. It is therefore desirable to have a heat conduction formulation that does not rely on a flux limiter. Such a formulation, which also accounts for nonlocal effects, is the convolution integral [17–19] formula. The use of convolution formulas is computationally simpler than the solution of the Boltzmann equation and is easily implemented in a hydrodynamic code. The usual convolution integral [17] for heat conduction is given by

$$Q_{NL}(\mathbf{r})=\int G(\mathbf{r},\mathbf{r}')Q_{SH}(\mathbf{r}')d\mathbf{r}', \tag{7}$$

where G is a kernel defined below. The physical basis behind Eq. (7) is that when the electron mean free path is long compared to the temperature gradient scale length, the heat flux at a position r is determined by the classical fluxes from other points r' up to a distance which corresponds to the mean free path of electrons having a velocity equal to $2.4\sqrt{T_e/m}$, which is characteristic of electrons dominating the heat flow [18]. Despite the fact that the above formula was not derived from first principles, it gives flux inhibition under sharp temperature gradients as well as preheat ahead of the main heat front and it leads to the classical Spitzer-Harm result in the diffusive limit. The kernel G in geometries other than planar would involve a complicated integral in three dimensions. For cylindrical geometry, an expression similar to the planar case is obtained by restricting the integral in Eq. (7) to a line through the central axis. A kernel for cylindrical geometry that takes into account the curvature and has the desirable property of giving a zero heat flux on axis and reduces to the planar case for large radii is given by

$$G(r,r')=\frac{1}{2a\lambda_e(r')}\times\exp\left[-\left|\frac{1}{aN_e(r')\lambda_e(r')}\int_{-\infty}^{\infty}N_e(r'')dr''\right|\right]\times\max[1,r'/r], \tag{8}$$

where $\lambda_e=(kT_e)^2/4\pi N_e e^4(Z^*+1)^{1/2}\ln\Lambda$ is the electron mean free path [17,18] and the numerical constant $a=32$

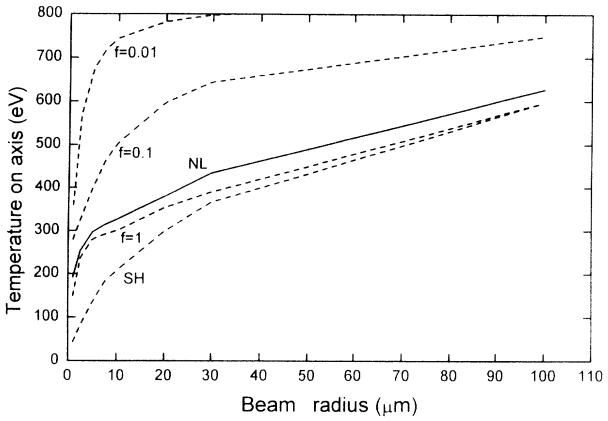

FIG. 2. Electron temperature on axis of a 100 Torr neon cylindrical target irradiated axially with a 0.268 μm, 12 ps (FWHM), 4×10^{17} W/cm^2 Gaussian (radially and temporally) laser pulse at the time of peak intensity as a function of beam radius (corresponding to $1/e$ of peak intensity). The curves given by the nonlocal (NL) heat conduction formula, flux limited diffusion (with $f=0.01$, 0.1, and 1), and diffusion with no flux limiter, as given by Spitzer and Harm (SH) are shown.

was chosen by Luciani, Mora, and Pellat [17] by comparison with more detailed calculations. The importance of heat conduction in determining the temperature at the center of the focus at the time of peak intensity of a 4×10^{17} W/cm^2, 12 ps full width at half maximum (FWHM) laser beam can be seen in Fig. 2. The target consists of 100 Torr neon and the laser has a Gaussian intensity profile in the radial direction. As the beam radius is reduced the temperature on axis decreases as a result of heat conduction. For very large radii the curves will merge together to a value given by zero heat conduction. For small radii the calculated temperature is very sensitive to the value of the flux limiter used. The nonlocal heat conduction model predicts a temperature intermediate between a flux limiter of 1 and 0.1 approximately. Heat conduction is only effective over time scales of the order of the electron diffusion time across the temperature gradient. This can be seen in Fig. 3, where the temperature on axis at the peak of the laser as calculated with and without heat conduction is shown as a function of pulse length for a 5 μm radius target. As the pulse length is reduced to about 1 ps, heat conduction becomes negligible on time scales of the order of the laser pulse length.

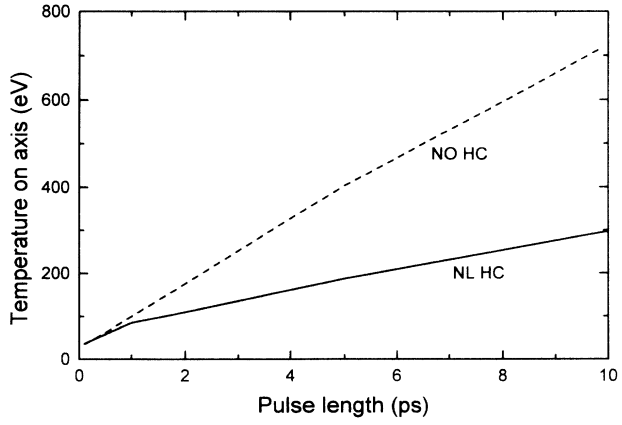

FIG. 3. Electron temperature on axis of a 100 Torr neon cylindrical target irradiated axially with a 5 μm radius, 0.268 μm wavelength, 4×10^{17} W/cm^2 peak intensity Gaussian (radially and temporally) laser pulse at the time of peak intensity as a function of pulse length (FWHM). The curves given by the nonlocal heat conduction (NL HC) formula and without heat conduction (NO HC) are shown.

III. SIMULATION OF 12 ps EXPERIMENTS

The model is used in this section to simulate the experiments on neon reported in Ref. [6]. The experiments were performed using the KrF laser facility at the Rutherford Appleton Laboratory. A 12 ps (FWHM) beam was focused to a spot of about 3.25 μm radius to give a peak intensity at the focus of about 4×10^{17} W/cm^2. The electron temperature was inferred from 90° Thomson scattering spectra of the laser beam and is therefore an average over the spatial region observed by the detector and also over the duration of the pulse. Since the laser pulse is approximately Gaussian in space and time the measurements are representative of conditions near the axis at the time of peak laser intensity because the scattering signal is proportional to the laser intensity and the electron density, which have their maxima on the axis of propagation of the laser beam at the time of peak intensity. In Fig. 4 we compare the experimental results for neon (from 1 to 100 Torr) with calculations employing different heat conduction models. Since the uncertainty on the experimental measurement is estimated to be about a factor of 2, there is good agreement with the nonlocal heat conduction model as well as a flux limited diffusion with $f\sim1$. The comparison is complicated by

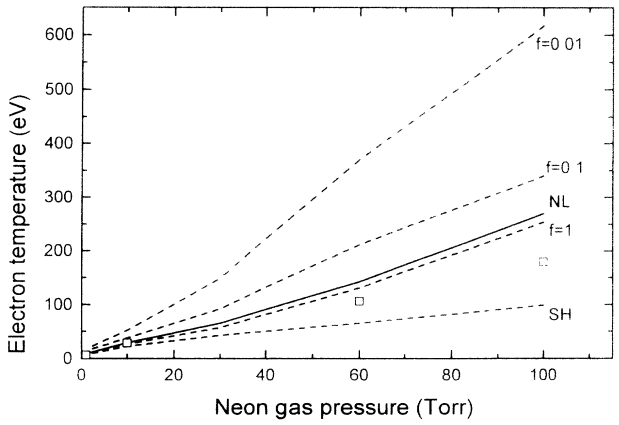

FIG. 4. Electron temperature on axis of a neon cylindrical target irradiated axially with a 3.25 μm radius, 0.268 μm wavelength, 4×10^{17} W/cm^2 peak intensity Gaussian (radially and temporally) laser pulse at the time of peak intensity as a function of gas pressure. Results from the nonlocal (NL) heat conduction, the Spitzer-Harm and flux limited diffusion (with $f=0.01$, 0.1, and 1), and diffusion with no flux limiter as given by Spitzer and Harm (SH) are shown. The squares show the experimentally measured data.

the temporal and spatial averaging of the detection system, as shown in the remainder of this section.

The time variation of the electron, ion temperature, and average ionization on axis is shown in Fig. 5. The ionization to the He-like stage is reached about 5 ps before the peak of the pulse since the peak intensity used in the calculation is approximately a factor of 2 higher than required to reach $Z^*=8$. Around the time of the peak of the laser intensity, the electron temperature is rising almost linearly, while the ionization is constant. The time averaged temperature should therefore be well approximated by the value at the time of peak intensity. The ion temperature is less than 1 eV since electron ion exchange is not effective at these low electron densities, high laser intensities, and short time scales.

The contributions to the electron temperature from ATI and IB are better seen in Fig. 6. For these long pulses and intensities ATI heating is negligible compared to IB. The plasma is heated by IB and cooled by thermal conduction. The electron temperature increases until 10 ps past the peak of the laser pulse, when thermal conduction cooling dominates the energy balance.

Another factor that can influence the averaging effect of the detection system is the radial distribution of the plasma parameters. The electron temperature and average ionization at the time of peak intensity as a function of radius are shown in Fig. 7. The use of a nonlocal heat conduction model results in a preheat front extending to about 80 μm. Flux limited diffusion with $f=0.5$ (chosen to give the same temperature on axis) shows a much sharper drop at a radius of about 20 μm. The He-like ionization region extends to a radius of 3 μm, where the electron temperature, as predicted by the two models, is constant. This flattening of the temperature on axis results from clamping of the central peak by efficient heat conduction.

Finally we investigate the effect of the ponderomotive force ($f_p=-N_e\nabla U_p$) [20] on the hydrodynamic motion of the plasma in the radial direction. This force is proportional to the radial gradients of the laser intensity and results in a force on the fluid (electrons plus ions) away from the central region. Figure 8 shows the electron density at the time of peak intensity with and without the ponderomotive force effects. The intensity profile is also shown. The effect of the ponderomotive force on the hydrodynamic motion is to reduce the density by up to a factor of 2 in the 3 μm radius region near the axis. As noted in Ref. [6], volume and time averaging effects of radially varying density will influence the scattered spectra, even though the temperature and laser intensity variations are small (see Fig. 7).

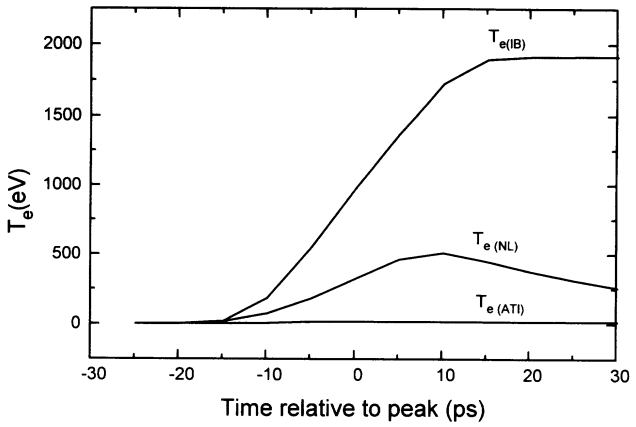

FIG. 6. Contribution to electron temperature in a 100 Torr neon cylindrical target from ATI ($T_{e(\mathrm{ATI})}$), IB ($T_{e(\mathrm{IB})}$), and the resulting temperature as calculated by the nonlocal heat conduction model ($T_{e(\mathrm{NL})}$) as a function of time relative to peak of intensity. The target is irradiated by a 3.25 μm radius, 0.268 μm wavelength, 4×10^{17} W/cm^2 peak intensity Gaussian (radially and temporally) laser pulse.

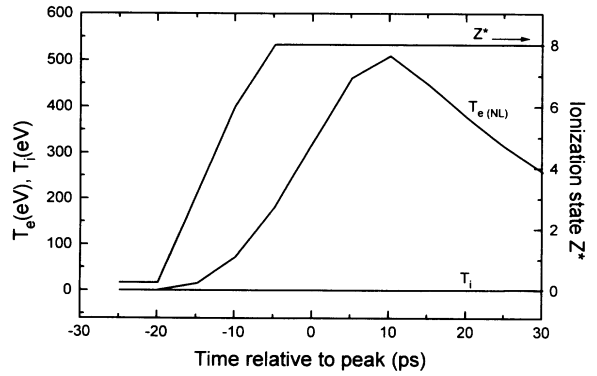

FIG. 5. Electron temperature from the nonlocal heat conduction model, ion temperature, and ionization state Z^* on the axis of a 100 Torr neon cylindrical target irradiated axially with a 3.25 μm radius, 0.268 μm wavelength, 4×10^{17} W/cm^2 peak intensity Gaussian (radially and temporally) laser pulse, as a function of time relative to peak of intensity.

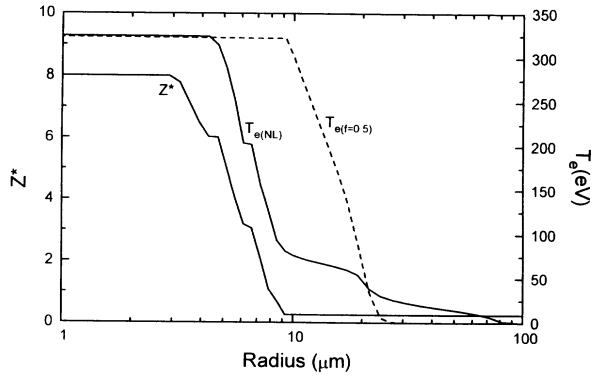

FIG. 7. Electron temperature in a 100 Torr neon cylindrical target as calculated from the nonlocal heat conduction model ($T_{e(\mathrm{NL})}$) and the flux limited diffusion ($T_{e(f=0.5)}$) at the time of peak intensity of a 3.25 μm radius, 0.268 μm wavelength, 4×10^{17} W/cm^2 peak intensity Gaussian (radially and temporally) laser pulse as a function of radius. Also shown is the average ionization Z^*.

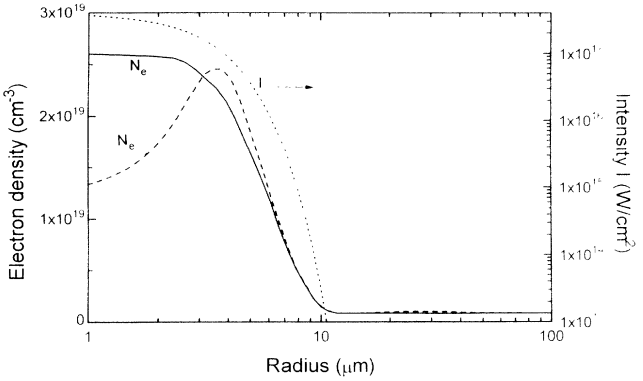

FIG. 8. Electron density in a 100 Torr neon gas target as calculated with the ponderomotive force (dashed curve) and without (full curve) at the time of the peak intensity of a 3.25 μm radius, 0.268 μm wavelength, 4×10^{17} W/cm^2 peak intensity Gaussian (radially and temporally) laser pulse as a function of radius. Also shown is the intensity profile (dotted curve).

IV. APPLICATION TO SHORTER PULSES AND HIGHER DENSITIES

The highest density used in the experiments described above corresponds to a He-like neon plasma with an electron density of 2.6×10^{19} cm^{-3}. This is about an order of magnitude lower than the densities envisaged for xuv lasers. Although the wavelength (0.268 μm) and intensity (4×10^{17} W/cm^2) used are adequate for the Li-like scheme described in Ref. [2], the pulse length (12 ps) is at least a factor of 50 longer than what is required. The effect of increasing the density and reducing the pulse length on the electron temperature at the end of the laser pulse (defined as 3 times the FWHM past the peak) is shown in Fig. 9. As the density increases the heating contribution from IB heating increases and results in a higher temperature at the end of the laser pulse. As the pulse length decreases the contribution from IB becomes negligible and only ATI contributes to the heating. The slight increase in temperature for the shortest pulse length is due a small increase in ionization intensity. A focal spot radius of 5 μm is used in these calculations and the effect of heat conduction can also be seen in Fig. 9, where the results for 1000 Torr neon without heat conduction are also shown. As expected, for subpicosecond pulses heat conduction is not effective on time scales of the order of the laser pulse length.

The temperature as calculated by our model for a 200 fs laser pulse at an intensity of 10^{18} W/cm^2, a wavelength of 0.248 μm, in a Ne^{8+} plasma at an electron density of 10^{20} cm^{-3} is shown in Fig. 10. The temperature at the end of the pulse is about 150 eV with a contribution from ATI of approximately 25 eV and the rest from inverse bremsstrahlung. This is in better agreement with Ref. [5], where a temperature of 200 eV was calculated, than with Ref. [4], where inverse bremsstrahlung was found to be negligible and an ATI temperature of 10 eV was calculated. Our calculated temperature is too high for the transient xuv laser scheme in Li-like neon proposed in Ref. [2], which requires a temperature <30 eV. Although this temperature might be achievable for pulse lengths <50 fs (see Fig. 9), no such pulses with sufficient energy to ionize the plasma have yet been produced. For the longer pulses available (>100 fs) additional cooling by heat conduction can be used to achieve inversion between excited states for quasi-steady-state recombination schemes. The rate of cooling for a cylinder with temperature T_e, electron density N_e, and radius r immersed in a cold background is approximately proportional to $T_e^{5/2}/(N_e r^2)$ and can be much higher than the adiabatic expansion cooling rate for a cylindrical plasma expanding

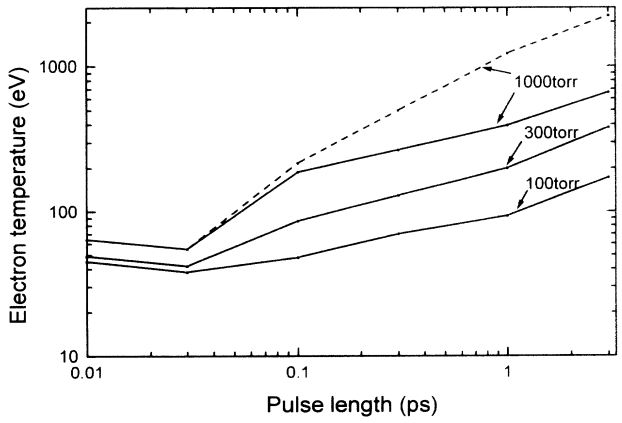

FIG. 9. Electron temperature on axis of a neon cylindrical target irradiated axially with a 5 μm radius, 0.268 μm wavelength, 4×10^{17} W/cm^2 peak intensity Gaussian (radially and temporally) laser pulse at the end of the laser pulse (taken as 3 times the FWHM past the peak of the pulse) as a function of pulse length (FWHM). Results of calculations using the nonlocal heat conduction model for 100, 300, and 1000 Torr (full curves) are shown. A calculation for 1000 Torr without any heat conduction is also shown (dashed curve).

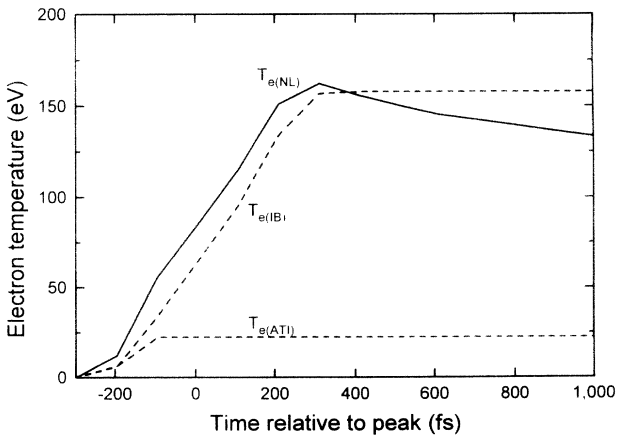

FIG. 10. Contributions to electron temperature in a He-like neon cylindrical target from ATI ($T_{e(\mathrm{ATI})}$), IB ($T_{e(\mathrm{IB})}$), and the resulting temperature given by the nonlocal heat conduction model ($T_{e(\mathrm{NL})}$) as a function of time relative to peak of intensity. The electron density is 10^{20} cm^{-3} and the target is irradiated by a 5 μm radius, 0.248 μm wavelength, 200 fs FWHM, 10^{18} W/cm^2 peak intensity Gaussian (radially and temporally) laser pulse.

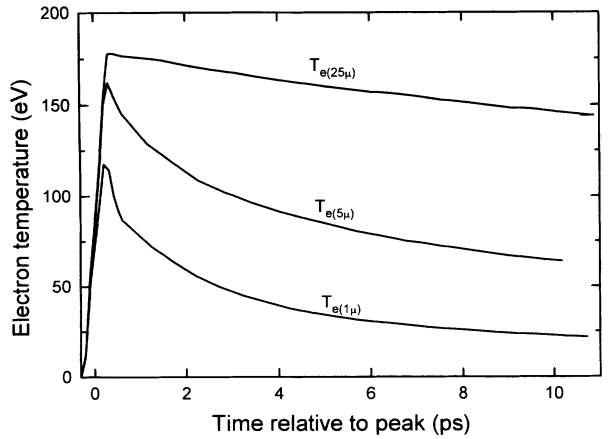

FIG. 11. Electron temperature in a He-like neon cylindrical filament as given by the nonlocal heat conduction model as a function of time relative to peak of intensity. The electron density is 10^{20} cm^{-3} and the target is irradiated by a 0.248 μm wavelength, 200 fs FWHM, 10^{18} W/cm^2 peak intensity Gaussian (radially and temporarily) laser pulse. Curves corresponding to 1, 5, and 25 μm radius are shown.

into vacuum, which is approximately proportional to $T_e^{1/2}/r$ [1]. Provided the difficulties associated with the production of long filaments of ionized plasma are resolved, it should be possible to control the rate of cooling by varying the radius of the filament. For small radii the cooling occurs on a time scale much smaller than the hydrodynamic time scale for expansion (>10 ps). This cooling by a supersonic heat wave is favorable for high gain at high electron densities and low temperatures. The time evolution of the electron temperature for the 200 fs case discussed above is shown in Fig. 11. The dependence of the cooling rate on radius is very strong at early times, but diminishes at later times as the heat front progresses to larger radii, in agreement with the simple scaling. Detailed calculations of small signal gain on $4\rightarrow3$ and $5\rightarrow3$ transitions in Li-like neon are in progress and will be reported in a forthcoming paper.

V. DISCUSSION

The electron temperature measurements based on Thomson scattering of the 12 ps KrF laser beam at a peak intensity of 4×10^{17} W/cm^2 focused to a 3.25 μm radius spot are well reproduced by a one-dimensional cylindrical hydrodynamic model which includes tunnel ionization, ATI, and nonlinear inverse bremsstrahlung heating as well as lateral heat conduction cooling. The electron temperature increases almost linearly with time before and after the peak of the laser beam, which provides a good justification for approximating the time average temperature by its value at the time of peak intensity. Heat conduction in the radial direction results in the clamping and flattening of the temperature profile near the axis. Heat conduction is only effective on time scales greater than a few picoseconds. For the conditions at the focus of the laser beam, the electron mean free is larger than the spatial extent of the focus and nonlocal effects are important. Inverse bremsstrahlung increases with both electron density and pulse length, but ATI heating is independent of both (ATI increases slightly for shorter pulses since ionization occurs at slightly higher intensity). ATI heating is negligible in the 12 ps experiment and the temperature is determined by a balance between IB heating and radial heat conduction cooling. Another important aspect of these OFI plasmas is the large difference between electron and ion temperature. At these densities, electron-ion energy exchanges are not effective on time scales of tens of picoseconds.

The application of the model to shorter pulses and higher densities relevant to the Li-like neon transient xuv scheme shows that for pulse lengths greater than 100 fs, inverse bremsstrahlung heating becomes important relative to ATI. A calculation for a 200 fs laser pulse at an intensity of 10^{18} W/cm^2, a wavelength of 0.248 μm, in a Ne^{8+} plasma at an electron density of 10^{20} cm^{-3}, gives a temperature of 150 eV at the end of the pulse, in reasonable agreement with Ref. [5]. The ATI contribution is only 25 eV and the rest is from IB. The contribution from IB can be minimized by using shorter pulses with the shortest pulse being determined by the requirement that there is enough energy in the pulse to ionize the plasma to the required state. The ATI contribution could also be minimized by removing the outermost electrons using a low intensity prepulse to preform a plasma channel, which is allowed to expand and cool, and then using a short intense pulse to ionize a filament to the final desired ionization state. At this stage it might be advantageous to use circularly polarized light so that the electrons ionized by the short pulse acquire a very high ATI energy and will not interfere with the recombination process on a transient recombination time scale (~1 ps).

Quasi-steady-state xuv schemes based on $4\rightarrow3$ or $5\rightarrow3$ transition in Li-like neon, for example, do not impose strict requirements on the electron temperature. Supersonic heat conduction is effective at cooling a plasma filament on a short time scale compared to quasi-steady-state inversion time scale (>10 ps) with little sensitivity to the initial temperature. The only problem in this case is the creation of a long plasma filament. For the high densities envisaged for xuv schemes, defocusing caused by rapid ionization would tend to disrupt the propagation of the beam over distances much longer than a Rayleigh distance. Preforming a plasma channel with a suitable electron density profile (see Fig. 7) to confine the short intense ionizing pulse has been suggested as a possible solution to the problem [1].

ACKNOWLEDGMENTS

We acknowledge useful discussions throughout this work with M. H. Key, W. Blyth, J. S. Wark, and S. G. Preston.

[1] N. H. Burnett and G. D. Enright, IEEE J. Quantum Electron. **26**, 1797 (1990).
[2] P. Amendt, D. C. Eder, and S. C. Wilks, Phys. Rev. Lett. **66**, 2589 (1991).
[3] For a review of the theory and experiments relating to collisional and recombination x-ray lasers, see R. C. Elton, *X-Ray Lasers* (Academic, San Diego, 1990); *X-Ray Lasers,* IOP Conf. Proc. No. 125 (Institute of Physics and Physical Society, London, 1992).
[4] B. M. Penetrante and J. N. Bardsley, Phys. Rev. A **43**, 3100 (1991).
[5] S. C. Rae and K. Burnett, Phys. Rev. A **46**, 2077 (1992).
[6] A. A. Offenberger, W. Blyth, A. E. Dangor, A. Djaoui, M. H. Key, Z. Najmudin, and J. S. Wark, Phys. Rev. Lett. **71**, 3983 (1994).
[7] A. Djaoui and S. J. Rose, J. Phys. B **25**, 2745 (1992).
[8] M. V. Ammosov, N. B. Delone, and V. P. Krainov, Zh. Eksp. Teor. Fiz. **91**, 2008 (1986) [Sov. Phys. JETP **23**, 924 (1966)].
[9] S. Augst, D. D. Meyerhofer, D. Strickland, and S. L. Chin, J. Opt. Soc. Am. B **8**, 858 (1991).
[10] N. H. Burnett and B. P. Corkum, J. Opt. Soc. Am. B **6**, 1195 (1989).
[11] T. W. Johnston and J. M. Dawson, Phys. Fluids, **5**, 722 (1973).
[12] V. P. Silin, Zh. Eksp. Teor. Fiz. **47**, 2254 (1964) [Sov. Phys. JETP **20**, 1510 (1965)].
[13] R. J. Faehl and N. F. Roderick, Phys. Fluids **21**, 793 (1978).
[14] L. Schlessinger and J. Wright, Phys. Rev. A **20**, 1934 (1979).
[15] A. Ya. Polishchuk and J. Meyer-Ter-Vehn, Phys. Rev. E **49**, 663 (1994).
[16] L. Spitzer and R. Harm, Phys. Rev. **89**, 977 (1953); L. Spitzer, Jr., *Physics of Fully Ionized Gases* (Wiley Interscience, New York, 1962).
[17] J. F. Luciani, P. Mora, and R. Pellat, Phys. Fluids **28**, 835 (1985).
[18] P. A. Holstein, J. Delettrez, and S. Skupsky, J. Appl. Phys. **60**, 2296 (1986).
[19] E. M. Epperlein and R. W. Short, Phys. Fluids B **3**, 3092 (1991).
[20] F. F. Chen, *Introduction to Plasma Physics and Controlled Fusion* (Plenum, New York, 1990).